ChemComm

COMMUNICATION

View Article Online
View Journal | View Issue

Cite this: *Chem. Commun.*, 2022, **58**, 10699

Received 17th June 2022,
Accepted 30th August 2022

DOI: 10.1039/d2cc03406a

rsc.li/chemcomm

A fluorescent probe strategy for the detection and discrimination of hydrogen peroxide and peroxynitrite in cells†

Hannah R. Bolland,[a] Ester M. Hammond[a] and Adam C. Sedgwick *[b]

Aryl boronate fluorescent probes allow the non-invasive study of dynamic cellular processes involving the reactive species, hydrogen peroxide (H_2O_2) and peroxynitrite ($ONOO^-$). However, the ability of these probes to differentiate between these two species remains unclear. Here, we report a boronate-functionalised hemicyanine dye (HD-BPin) as a potential strategy to distinguish between H_2O_2 at 704 nm (red channel) and $ONOO^-$ at 460 nm (blue channel) in solution and in cells. This work also highlights the choice of fluorophore before boronate functionalization can dictate the observed selectivity between these two species.

Hydrogen peroxide (H_2O_2) and peroxynitrite ($ONOO^-$) are reactive oxygen (ROS) and reactive nitrogen species (RNS) found within living systems.[1] Both species have been identified as key signaling molecules that regulate a variety of cellular processes, ranging from cell growth, differentiation, migration, and programmed cell death.[2–4] These chemical biomarkers also act as a source of oxidative and nitrosative stress, in which aberrant concentrations lead to the irreversible modification of important biomolecules such as proteins, enzyme, lipids, and DNA.[2,5] The results of these pathological effects are linked to several diseases including cancer, cardiovascular disease, and neurodegenerative disease.[6,7] For these reasons, extensive efforts have been devoted to developing methods that can provide detailed information on these species in biological settings.[8] However, at present the specific identification of these individual RNS and ROS has proved challenging. Here, we report the fluorescent probe **HD-BPin** as a potential strategy for the detection of H_2O_2 (704 nm) and $ONOO^-$ (460 nm) in aqueous solution and cells. The key feature of this strategy is that it takes advantage of differences in kinetic reactivity and emission wavelengths to signal the presence of each species.

Small-molecule fluorescent probes have emerged as powerful chemical tools that allow the non-invasive and real-time imaging of cellular processes and biological species.[9] Pioneering work by the groups of Chang, Czarnik, Shabat, Lippard, and Tsien, among many others, exploited various aspects of molecular recognition and synthetic methodology to develop a suite of fluorescent probes with high level of specificity for various biological species, including ROS/RNS, biomolecules, and metal ions.[9,10] However, as the field has grown, it has become apparent that these first- and second-generation systems built off various fluorescent scaffolds (*e.g.*, coumarin, xanthene, and BODIPY) have limitations.[11] For example, a first-generation H_2O_2-responsive fluorescent probe, peroxyresorufin-1 (PR1), has recently been reported to respond to $ONOO^-$.[12,13] This observed reactivity is due to the faster reaction kinetics of $ONOO^-$ compared to H_2O_2 for aryl boronates.[14] As a result, this functionality is now being increasingly used for the selective detection of $ONOO^-$.[14–16] However, with H_2O_2-selective aryl boronate probes still being reported,[17] we rationalized that the choice of fluorescent scaffold may play a role in dictating selectivity between H_2O_2 and $ONOO^-$ and therefore, we believed a strategy to distinguish these two species could be potentially identified. This study was undertaken in an effort to test this hypothesis.

Cyanine (Cy) and hemicyanine (HD)-based fluorophores have found extensive use in the design of fluorescent-based and photoacoustic-based chemical sensors.[18–20] Many of these reported systems employ the boronate functionality to detect H_2O_2 *in vitro* and *in vivo*.[21–23] This observed H_2O_2 selectivity is unexpected due to the greater reactivity of $ONOO^-$ for aryl boronates.[14] Previous studies suggest that $ONOO^-$ reacts *via* the oxidative cleavage of the methine bridges (Fig. 1 – blue box) rather than the expected boronate oxidation (Fig. 1 – red box).[24,25] We thus hypothesized boronate-based Cy- or HD-probes may provide the ability to discriminate between H_2O_2 and $ONOO^-$. To test this hypothesis, we synthesized and evaluated two boronate-based fluorescent probes, **HD-BPin** and **Cy7-BPin** (Fig. 1) – see supporting information for synthetic procedures (ESI,† Scheme S1 and S2).

[a] *Oxford Institute for Radiation Oncology, Department of Oncology, University of Oxford, Old Road Campus Research Building, Oxford, OX3 7DQ, UK*
[b] *Chemistry Research Laboratory, University of Oxford, Mansfield Road, OX1 3TA, UK. E-mail: adam.sedgwick@chem.ox.ac.uk*

† Electronic supplementary information (ESI) available. See DOI: https://doi.org/10.1039/d2cc03406a

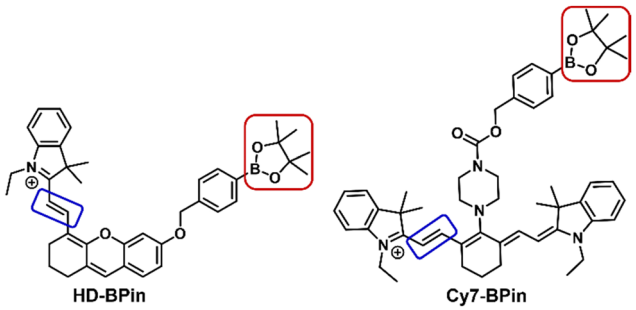

Fig. 1 Chemical structures of **HD-BPin** and **Cy7-BPin**. Red box highlights H_2O_2 and $ONOO^-$ reactive aryl boronate motif. Blue box highlights $ONOO^-$ reactive methine bridge.

With **HD-BPin** and **Cy7-BPin** (Fig. 1) in hand, we first tested the response of each probe to H_2O_2 and $ONOO^-$ in aqueous solution (PBS buffer, pH 7.2). As expected, the addition of H_2O_2 resulted in increases in the intensity of the near-infrared (NIR) fluorescence features (red emission) at 704 nm and 780 nm for **HD-BPin** and **Cy7-BPin**, respectively (Fig. 2A and ESI,† Fig. S1).[7,8] These observations are consistent with previous reports (see ESI,† Schemes S3 and S4 for proposed reaction mechanisms).[21,22,26] Changes in the absorption profiles of **HD-BPin** and **Cy7-BPin** were also seen (ESI,† Fig. S2 and S3). In contrast, the addition of $ONOO^-$ (100 μM) to **Cy7-BPin** resulted in a dramatic change to its NIR absorption with a significant decrease at 750 nm and an appearance of a new absorption peak at ~525 nm. Unfortunately, no new fluorescent species were observed, which suggests degradation of the cyanine dye scaffold (ESI,† Fig. S4 and S5). Because of this, it was no longer a focus for the rest of the study. With the addition of $ONOO^-$ (100 μM) to **HD-BPin**, an immediate color change from blue to colorless was observed (ESI,† Fig. S6). This color change was also accompanied by a rapid increase in blue fluorescence emission intensity at 460 nm (λ_{ex} = 360 nm, ESI,† Fig. S7), which is consistent with the $ONOO^-$-mediated formation of a blue fluorescent xanthene dye[24,27] – see ESI† for proposed reaction mechanism (ESI,† Scheme S5). Combined with previous reports on aryl boronate fluorescent probes (*e.g.*, PR1 and peroxyorange-1[28] (ESI,† Fig. S8 and S9)), this data shows the choice of fluorophore when designing a probe has potential to dictate the observed selectivity between H_2O_2 and $ONOO^-$.

Next, we turned our attention to the evaluation of the dual-wavelength response of **HD-BPin** as a potential strategy for distinguishing H_2O_2 and $ONOO^-$ in solution and in cells. Increasing H_2O_2 concentrations (0–450 μM) resulted in a dose-dependent increase at 704 nm with a calculated limit of detection (LOD) = 2.10 μM (Fig. 2A and ESI,† Fig. S10 and S11). Oxidation of the boronate functionality affording the red emissive species was confirmed by mass spectrometry (ESI,† Fig. S12). These responses required incubation times of >30 mins and an overall >20-fold change in red fluorescence emission intensity was observed (Fig. 2B and ESI,† Fig. S13). To our satisfaction, minimal changes in blue fluorescence emission intensity were observed, even at high H_2O_2 concentrations (*i.e.*, 200 and 400 μM) (ESI,† Fig. S14–S16).

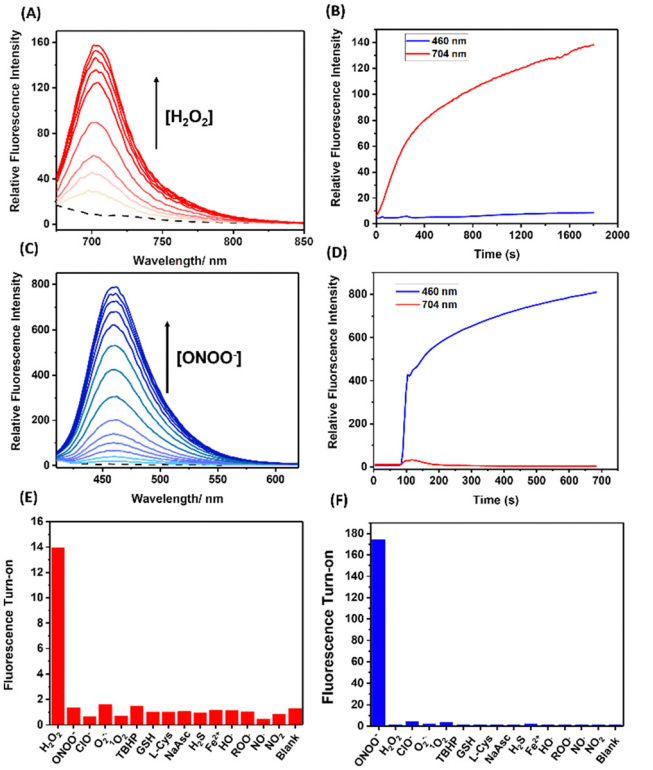

Fig. 2 (A) Fluorescent spectra of **HD-BPin** (10 μM) with increasing concentrations of H_2O_2 (0–450 μM, λ_{ex} = 660 nm, 30 min incubation). (B) Changes in relative fluorescence intensity of **HD-BPin** (10 μM) at 704 nm (Red) and at 460 nm (Blue) in the presence of H_2O_2 (200 μM), λ_{ex} = 660 nm (Red)/λ_{ex} = 360 nm (Blue). (C) Fluorescence spectra of **HD-BPin** (10 μM) with increasing concentrations of $ONOO^-$ (0–140 μM, λ_{ex} = 360 nm). (D) Changes in relative fluorescence intensity of **HD-BPin** (10 μM) at 704 nm (Red) and at 460 nm (Blue) in the presence of $ONOO^-$ (100 μM), λ_{ex} = 660 nm (Red)/λ_{ex} = 360 nm (Blue). (E) Reaction selectivity of **HD-BPin** (10 μM) with biologically relevant species (100 μM each species) at 704 nm (λ_{ex} = 660 nm). (D) Reaction selectivity of **HD-BPin** (10 μM) with biologically relevant species (100 μM each species) at λ_{ex} = 360 nm. All measurements were performed in PBS buffer solution pH = 7.20. Slit widths: 10 nm and 5 nm.

In contrast, the addition of $ONOO^-$ (0–140 μM) resulted in a significant increase in fluorescence intensity at 460 nm with a calculated LOD = 0.28 μM (Fig. 2C and ESI,† Fig. S17). These $ONOO^-$ induced responses required less than 30 s and an overall ~200-fold increase in blue fluorescence was observed (Fig. 2D). At low $ONOO^-$ concentrations (0–15 μM), an initial increase in blue and red emission intensity was observed. However, when $ONOO^-$ concentrations exceeded >10 μM, the fluorescence emission intensity at 704 nm decreased while the blue emission continued to increase in intensity (ESI,† Fig. S18 and S19). This observation suggests a stepwise deprotection mechanism, in which boronate oxidation is favored before the oxidation of the methine bridge (ESI,† Scheme S6). This potential stepwise mechanism is supported by the sigmoidal curve seen in titration experiments and mass spectroscopic analysis identifying the presence of both red and blue emissive species (ESI,† Fig. S21–S24). Although this increase in red emission was unexpected, this turn on response can be readily differentiated from

H_2O_2 due to the simultaneous increase in blue emission intensity at 460 nm. Together, these results demonstrate that **HD-BPin** can differentiate between H_2O_2 and $ONOO^-$ responses in solution through differences in kinetics ($ONOO^-$ (seconds) and H_2O_2 (minutes)) and differences in emission intensities at 704 nm and 460 nm. Before evaluating this strategy in cell studies, a selectivity assay was carried out against other ROS/RNS, reductants and thiols. As seen in Fig. 2E and F, excellent selectivity was observed for H_2O_2 at 704 nm and for $ONOO^-$ at 460 nm (Fig. 2E and F).

Incubation of **HD-BPin** in A549 cells was shown not to impact cell viability (ESI,† Fig. S25). Subsequently, we evaluated the fluorescence response of **HD-BPin** in A549 cells *via* fixed cell imaging with the exogenous addition of H_2O_2 and SIN-1[29] ($ONOO^-$ donor). SIN1 (500 μM) treatment led to an increase in blue fluorescence with its maximum intensity at 30 minutes (2.5-fold increase compared to time zero, Fig. 3A). No significant changes in red emission were observed over the measured time points (0–80 mins). Although a slight decrease in blue fluorescence emission can be observed after the optimal 30 min timepoint, the overall fluorescence emission intensity still differs in a statistically significant manner from untreated cells incubated with **HD-BPin** only. H_2O_2 treatment (100 μM) resulted in an expected time-dependent increase with an overall 8.6-fold increase in red fluorescence emission after 80 mins (Fig. 3B). Consistent with solution data, minimal changes in emission intensity were seen in the blue emission channel. Scavengers, ebselen (Ebs., $ONOO^-$ scavenger) and catalase (Cat., H_2O_2 scavenger) confirmed the specificity of each observed signal (Fig. 3A and B). Similar trends were observed for **HD-BPin** when tested in H460 and HCT116 cell lines (ESI,† Fig. S26 and S27). Since 1–3% of SIN1 concentration is reported to form peroxynitrite,[30] we wanted to test the response of **HD-BPin** to various SIN1 and H_2O_2 concentrations. As shown in Fig. S28 (ESI†), increasing SIN1 concentrations (0–1500 μM) resulted in an initial increase in both blue and red emission intensity followed by a further increase in blue emission with a concomitant decrease in emission in the red channel, reflecting the obtained cuvette data. Whereas, increasing H_2O_2 concentrations (0–300 μM, 80 min incubation) led to a dose-dependent increase in the red channel with minimal increases in blue emission (ESI,† Fig. S29). It is important to note at low H_2O_2 and $ONOO^-$ concentrations differences between blue and red emission are less substantial and therefore one should take caution during cell analysis.

To demonstrate the potential utility of this strategy, **HD-BPin** was evaluated in A549 cells treated with known ROS inducers, which include cisplatin, menadione and antimycin A.[31,32] Current literature reports suggest H_2O_2 contributes to cisplatin-mediated cell death.[33] Interestingly, as seen in Fig. S30 and S31 (ESI†), the

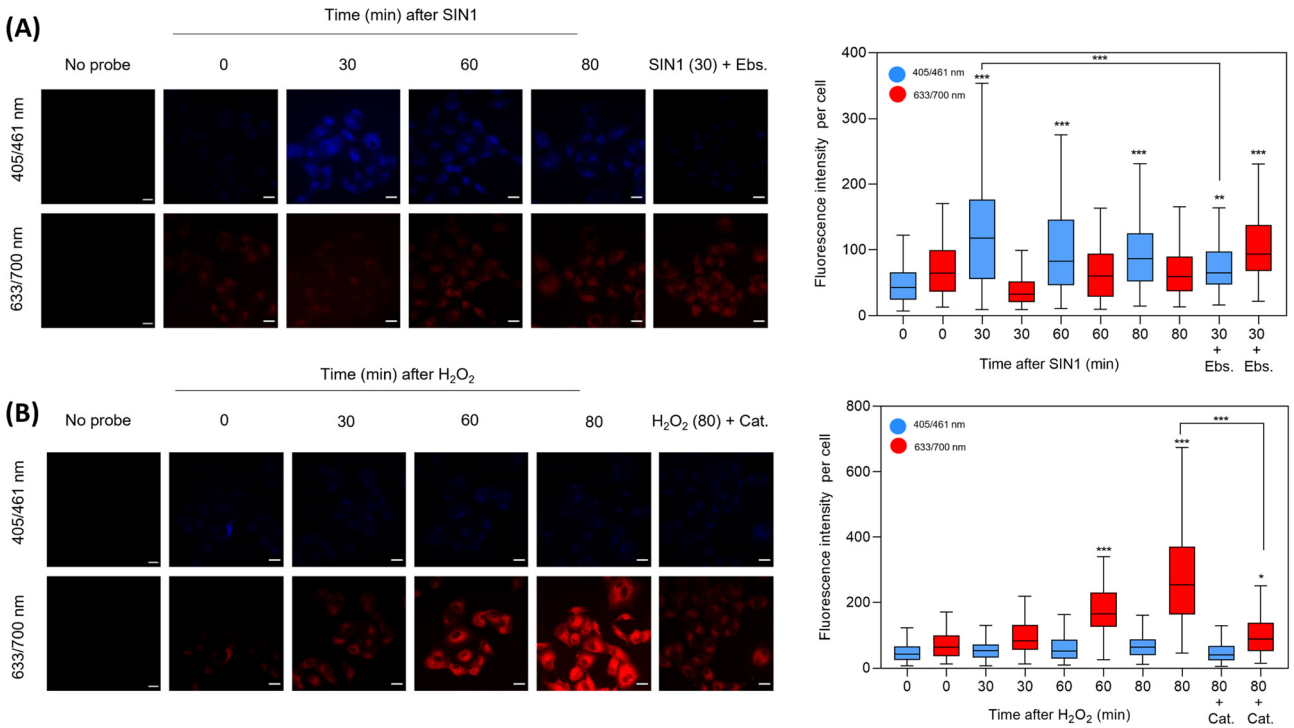

Fig. 3 Fluorescence images of A549 cells incubated with **HD-BPin** (10 μM) followed by addition of SIN-1 or H2O2. A549 cells were pre-treated with **HD-BPin** (10 μM) and then treated with either (A) SIN1 (500 μM) or (B) H_2O_2 (100 μM) and fixed at the indicated times. For scavenging experiments, cells were pre-treated for 4.5 hours with either Ebselen (10 μM, Ebs.) to scavenge $ONOO^-$ or Catalase (1000 U mL^{-1}, Cat.) to scavenge H_2O_2. Representative images of time points taken at 405/461 nm to visualise changes in blue emisison and 633/700 nm to visualise changes in red emission. Scale bar represents 20 μm. Images taken at 63x magnification. (Quantification data is fluorescence intensity per cell, black line indicates mean. For each condition 100 cells were imaged and quantified. Outliers were excluded using Tukeys box plot. Error bars represent SD. Significance tested *via* One way ANOVA. * $p < 0.05$ ** $p < 0.01$ and *** $p < 0.001$. $n = 3$.

obtained images suggest an increase in $ONOO^-$ production as time progressed in A459 cells treated with cisplatin (15 μM). Exogenous addition of Cat. (H_2O_2) and Ebs. ($ONOO^-$) resulted in decreases in the respect red and blue emission suggesting presence of both H_2O_2 and $ONOO^-$. PO1 was used as a comparison (ESI,† Fig. S32). A549 cells treated with menadione and antimycin A showed a dose-dependent increase in red emission with little changes seen in the blue emission channel (ESI,† Fig. S33 and S34). This observation suggests a sole increase in intracellular H_2O_2. These image profiles shows this present strategy has the potential to provide greater molecular insight and overcome the limitations of current commercially available aryl boronate fluorescent probes (*e.g.*, PO1).

In summary, this report demonstrates the fluorescent probe **HD-BPin** as a potential strategy to distinguish between H_2O_2 and $ONOO^-$ in solution and in cells. Differences in kinetics and resultant emission intensities successfully enables the ability to distinguish between a H_2O_2 induced response and $ONOO^-$ induced response. However, at low $ONOO^-$ and H_2O_2 concentrations, the user should take caution when evaluating differences in both red and blue channels in cells. We anticipate this report to be a useful guide for the development of future ROS/RNS fluorescent probes when using the aryl boronate motif.

ACS would like to thank the Glasstone Research fellowship (University of Oxford) and the major research grant from Jesus College Oxford for financial support. ACS would like to acknowledge the support of Professor Stuart Conway and Professor Stephen Faulkner. HB and EMH thank the EPSRC for the support of programme grant EP/S019901/1.

Conflicts of interest

There are no conflicts of interests to declare.

References

1 E. A. Veal, A. M. Day and B. A. Morgan, *Mol. Cell*, 2007, **26**, 1–14.
2 H. Sies, *Redox Biol.*, 2017, **11**, 613–619.
3 P. Pacher, J. S. Beckman and L. Liaudet, *Physiol. Rev.*, 2007, **87**, 315–424.
4 C. Szabó, H. Ischiropoulos and R. Radi, *Nat. Rev. Drug Discovery*, 2007, **6**, 662–680.
5 S. Bartesaghi and R. Radi, *Redox Biol.*, 2018, **14**, 618–625.
6 M. P. Lisanti, U. E. Martinez-Outschoorn, Z. Lin, S. Pavlides, D. Whitaker-Menezes, R. G. Pestell, A. Howell and F. Sotgia, *Cell Cycle*, 2011, **10**, 2440–2449.
7 E. Gochman, J. Mahajna and A. Z. Reznick, *Anticancer Res.*, 2011, **31**, 1607–1617.
8 Y. Zhang, M. Dai and Z. Yuan, *Anal. Methods*, 2018, **10**, 4625–4638.
9 D. Wu, A. C. Sedgwick, T. Gunnlaugsson, E. U. Akkaya, J. Yoon and T. D. James, *Chem. Soc. Rev.*, 2017, **46**, 7105–7123.
10 K. J. Bruemmer, S. W. M. Crossley and C. J. Chang, *Angew. Chem., Int. Ed.*, 2020, **59**, 13734–13762.
11 J. Chan, S. C. Dodani and C. J. Chang, *Nat. Chem.*, 2012, **4**, 973–984.
12 M. Weber, A. B. Mackenzie, S. D. Bull and T. D. James, *Anal. Chem.*, 2018, **90**, 10621–10627.
13 E. W. Miller, A. E. Albers, A. Pralle, E. Y. Isacoff and C. J. Chang, *J. Am. Chem. Soc.*, 2005, **127**, 16652–16659.
14 A. Sikora, J. Zielonka, M. Lopez, J. Joseph and B. Kalyanaraman, *Free Radical Biol. Med.*, 2009, **47**, 1401–1407.
15 N. Rios, L. Piacenza, M. Trujillo, A. Martinez, V. Demicheli, C. Prolo, M. N. Alvarez, G. V. Lopez and R. Radi, *Free Radical Biol. Med.*, 2016, **101**, 284–295.
16 J. Zielonka, A. Sikora, J. Joseph and B. Kalyanaraman, *J. Biol. Chem.*, 2010, **285**, 14210–14216.
17 J. Hou, M. Qian, H. Zhao, Y. Li, Y. Liao, G. Han, Z. Xu, F. Wang, Y. Song and Y. Liu, *Anal. Chim. Acta*, 2018, **1024**, 169–176.
18 S. H. Gardner, C. J. Brady, C. Keeton, A. K. Yadav, S. C. Mallojjala, M. Y. Lucero, S. Su, Z. Yu, J. S. Hirschi, L. M. Mirica and J. Chan, *Angew. Chem., Int. Ed.*, 2021, **60**, 18860–18866.
19 Y. Tan, L. Zhang, K. H. Man, R. Peltier, G. C. Chen, H. T. Zhang, L. Y. Zhou, F. Wang, D. Ho, S. Q. Yao, Y. Hu and H. Y. Sun, *ACS Appl. Mater. Interfaces*, 2017, **9**, 6796–6803.
20 J. Yin, Y. Kwon, D. Kim, D. Lee, G. Kim, Y. Hu, J. H. Ryu and J. Yoon, *J. Am. Chem. Soc.*, 2014, **136**, 5351–5358.
21 J. Weber, L. Bollepalli, A. M. Belenguer, M. D. Antonio, N. De Mitri, J. Joseph, S. Balasubramanian, C. A. Hunter and S. E. Bohndiek, *Cancer Res.*, 2019, **79**, 5407–5417.
22 J. Zhang, L. Shi, Z. Li, D. Li, X. Tian and C. Zhang, *Analyst*, 2019, **144**, 3643–3648.
23 Y. Hao, Z. Li, N. Ding, X. Tang and C. Zhang, *Spectrochim. Acta, Part A*, 2022, **268**, 120642.
24 D. Y. Zhou, O. Y. Juan, Y. Li, W. L. Jiang, T. Yang, Z. M. Yi and C. Y. Li, *Dyes Pigm.*, 2019, **161**, 288–295.
25 T. Hou, K. Zhang, X. Kang, X. Guo, L. Du, X. Chen, L. Yu, J. Yue, H. Ge, Y. Liu, A. M. Asiri, K. A. Alamry, H. Yu and S. Wang, *Talanta*, 2019, **196**, 345–351.
26 A. Sagi, R. Weinstain, N. Karton and D. Shabat, *J. Am. Chem. Soc.*, 2008, **130**, 5434.
27 L. L. Wu, J. H. Liu, X. Tian, R. R. Groleau, S. D. Bull, P. Li, B. Tang and T. D. James, *Chem. Sci.*, 2021, **12**, 3921–3928.
28 B. C. Dickinson, C. Huynh and C. J. Chang, *J. Am. Chem. Soc.*, 2010, **132**, 5906–5915.
29 I. M. Bonilla, A. Sridhar, Y. Nishijima, S. Gyorke, A. J. Cardounel and C. A. Carnes, *J. Cardiovasc. Pharmacol.*, 2013, **61**, 401–407.
30 F. J. Martin-Romero, Y. Gutierrez-Martin, F. Henao and C. Gutierrez-Merino, *J. Fluoresc.*, 2004, **14**, 17–23.
31 G. Loor, J. Kondapalli, J. M. Schriewer, N. S. Chandel, T. L. Vanden Hoek and P. T. Schumacker, *Free Radical Biol. Med.*, 2010, **49**, 1925–1936.
32 W. H. Park, Y. W. Han, S. H. Kim and S. Z. Kim, *J. Cell. Biochem.*, 2007, **102**, 98–109.
33 Y. I. Chirino and J. Pedraza-Chaverri, *Exp. Toxicol. Pathol.*, 2009, **61**, 223–242.

